Hindawi
Shock and Vibration
Volume 2018, Article ID 6863176, 14 pages
https://doi.org/10.1155/2018/6863176

Research Article

Transmission Error Analysis and Disturbance Optimization of Two-Stage Spur Gear Space Driven Mechanism with Large Inertia Load

Jianfeng Ma, Chao Li, and Lingli Cui

Key Laboratory of Advanced Manufacturing Technology, Beijing University of Technology, Chao Yang District, Beijing 100124, China

Correspondence should be addressed to Jianfeng Ma; 18612648241@163.com and Lingli Cui; acuilingli@163.com

Received 4 November 2017; Revised 20 March 2018; Accepted 2 April 2018; Published 13 June 2018

Academic Editor: Dario Di Maio

For the nonlinear disturbance actual issues of the model space drive mechanism two-stage spur gear system, a nonlinear dynamic model of 14-DOF (degree of freedom) two-stage spur gear with time-varying stiffness and damping was established. This model has been developed previously by the authors to access the large inertia on the dynamic response of spur gear space driving mechanism, and its effectiveness was proved by a motion simulation experiment. In this paper, the profile error (PE) and the index error (IE) were enhanced in the dynamic model. The effects of profile error, index error, and variable load torque on transmission error (TE) were analyzed, while the optimization was proposed according to the analyzed result. The peak-to-peak value of the optimized load transmission error (LTE) was reduced by 60.7%, which improved the transmission accuracy and reduced the phenomenon of disturbance. The research of nonlinear dynamical model of two-stage spur gear and the TE of the large inertia load were enriched, which provided an important reference for the actual design of the gear system.

1. Introduction

The gear transmission system is widely utilized in machine tools, aerospace application, ships, and wind power as well as in other fields. It is of great significance to perform dynamic modeling and failure mechanism analysis on key parts of gearbox such as gears and bearings [1–3]. The large inertia load in the space drive system has a significantly wide range of applications, because the load inertia of the entire system is relatively high compared to the transmission part, posing new problems and challenges in the transmission accuracy, life, reliability, and safety of the spacecraft transmission system. The main difference between the gear system and other mechanical systems is the corresponding internal excitation. Three types of internal excitation exist in the gear system: stiffness excitation, error excitation, and meshing shock excitation. The PE and IE caused by gear machining are the main error incentives for the gear system.

At present on the gear system modeling, it is necessary to establish a nonlinear time-varying dynamic model including time-varying stiffness [4] and transmission error. Junguo Wang [5] studied the torsional vibration model of a single-stage spur gear drive system, analyzing the effect of stiffness on the dynamic behavior of the locomotive gear transmission system. Lassâad Walha [6] and Kamel Abboudi [7] established a 12-DOF nonlinear dynamic model for the two-stage gear system, only considering the gear system itself without the effects of input and output in the model. Parker [8, 9] and Fernández [10] established a finite element model of gear transmission, based on the finite element contact mechanics theory. Wu [11] established a dynamic finite element model of the gear transmission system based on finite element analysis software. To improve the accuracy of time-varying mesh stiffness, a universal gear profile equation that references the actual manufacturing process was applied to calculate the meshing stiffness by Lingli Cui [12].

The analysis of the dynamic characteristics of the large inertia load space drive mechanism is less relevant in the theoretical research, which mainly utilizes simulation technology for both analysis and research. Tianfu Yang [13] considered the impact of a high reduction ratio and studied the dynamic characteristics of the space manipulator, whereas

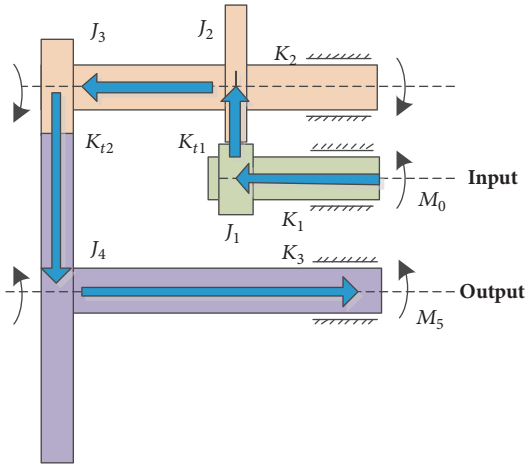

Figure 1: Diagram of two-stage gear transmission.

the characteristics of the large inertia load were not analyzed. Zhigang Xu [14] proposed an equivalent simulation method for an excessively large inertia load, simulating the large moment of inertia required by the space manipulator and verified the effectiveness of the method by numerical simulation under different working conditions. Chen Shiqi [15] established a bending-torsion coupling nonlinear dynamic model of a low speed overload planetary gear drive system with friction and studied the effect of friction on the nonlinear dynamic behavior of a low speed overload gear transmission. Ahmed Hammami [16] developed a model of planetary gear torsional concentrated parameter with dynamic recirculation and studied the nonlinear behavior under variable load conditions. In this paper, the large inertia load space drive mechanism gear reduction system was utilized for the driving of a satellite sun wing. Since the sun wing is required to be changed in real time, according to the position of the sun, the mechanism is required to start and stop frequently at low speed. An apparent phenomenon of disturbance when the mechanism is stopped exists. Therefore in this paper, the effects of large inertia load torque on the system were focused on.

The effects of error incentives on the system and the relationship between the gear machining errors and the system dynamic characteristics can provide guidance for the determination of the accuracy grade in the gear design and the selection of the machining method. Fernández [17, 18] added profile and pitch errors in the dynamic model, executing tooth profile modification, and validated the validity of the model through the examples simulation under different torques. A gear dynamics test set-up with integrated root strain and dynamic transmission error measurement systems was described by M.A. Hotait [19], in which dynamic factor and dynamic transmission error measurements from both unmodified and modified spur gears were presented and the corresponding relationship was demonstrated experimentally. Tengjiao Lin [20] utilized the finite element modeling to obtain the machining and assembly errors of the gear system, which was applied to the kinetic model, and the dynamic transmission error was calculated. Guangjian Wang [21] proposed the theoretical calculation equation of the no-load transmission error and studied the load variation frequency effect on the transmission error curve.

On the basis of extensive reading relevant literature, in certain studies, the no-linear factors such as PE and IE in the dynamic model were not considered, whereas in other studies the TE of the system was not analyzed. Moreover, in other studies, the large inertia load was not taken into account. For these deficiencies, in this article, the effects of various factors were considered as much as possible, and the simulation model and the actual operation of the gear were attempted to be made consistent. To improve the gear system transmission accuracy and reduce the disturbance of the gear system, the gear reduction system of the large inertia load space drive mechanism was considered as the research object. The dynamic model of the gear system was established, where it was analyzed by static and dynamic analysis methods. The results were achieved through the effects analysis of all PE, IE, and load torque on the TE. Then, the machining accuracy grade and input torque of the gear system were optimized, according to the analysis results.

2. Nonlinear Dynamic Model of Two-Stage Gear

The dynamic modeling of a two-stage spur gear reduction system for a large inertia load space drive mechanism was carried out. In this case, the quality, the moment of inertia, the radius, and the average meshing stiffness of each gear were assumed to be evenly distributed along the center wheel, and the system damping was assumed to be elastic damping. The mutual sliding between the teeth was ignored, whereas the engaging force acted in the meshing surface and perpendicularly to the tooth contact line. The system was simplified, as presented in Figure 1. The power transmission process is represented by the blue arrow.

The motor was connected to the input of the input axis, where the input axis torsional stiffness was K_1 and the

Table 1: Two-stage gear drive system parameters.

Gear pair 1		Gear pair 2	
Number of teeth of gear 1	18	Number of teeth of gear 3	18
Number of teeth of gear 2	90	Number of teeth of gear 4	360
Modulus of gear 1	0.25mm	Modulus of gear 3	0.5mm
Modulus of gear 2	0.25mm	Modulus of gear 4	0.5mm
Material of gear 1	stainless steel	Material of gear 3	stainless steel
Material of gear 2	Titanium alloy	Material of gear 4	Titanium alloy
Accuracy level	6-h	Accuracy level	6-h
Tolerance of cycle accumulated deviations of gear 1	0.016mm	Tolerance of cycle accumulated deviations of gear 3	0.016mm
Tolerance of cycle accumulated deviations of gear 2	0.02mm	Tolerance of cycle accumulated deviations of gear 4	0.032mm
Tolerance of PE of gear 1	0.008mm	Tolerance of PE of gear 3	0.008mm
Tolerance of PE of gear 2	0.008mm	Tolerance of PE of gear 4	0.006mm

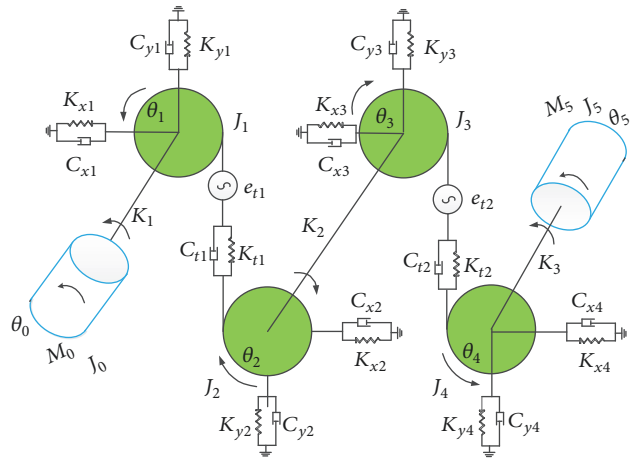

Figure 2: Dynamic model of two-stage gear transmission system.

input torque of the motor was M_0. The output axis torsional stiffness was K_3 and the resistance torque of the output load was M_5. The rotational inertia of the four gears of the gear system was J_1, J_2, J_3, and J_4. The time-varying meshing stiffness between gears 1 and 2 was K_{t1}, while between gears 3 and 4 it was K_{t2}. The mid axis torsional stiffness between gears 2 and 3 was K_2.

The parameters of the two-stage gear drive system are presented in Table 1.

With the time-varying meshing stiffness of the two-stage gear system, the radial displacement of the gears, and the PE and IE consideration, to establish the dynamic model of the system, the following assumptions were utilized:

(1) The bearing friction was ignored, where only in the load side a load resistance torque was added.

(2) The input torque of the motor was assumed to be constant and the torque ripple was ignored.

(3) Gear engaging force was always in the direction of the meshing line.

The torsional vibration model of the 14-DOF two-stage spur gear system is presented in Figure 2, including the torsional displacement vibration in 6 directions and the radial displacement vibration in 8 directions.

According to Newton's second law and the related dynamics knowledge, the dynamic equations of the aforementioned two-stage spur gears are established as follows. Reader should check previous works, such as [22], for a more detailed description of the dynamic model and its validation.

$$\mathbf{m}\ddot{\mathbf{x}} + \mathbf{c}_0\dot{\mathbf{x}} + \mathbf{k}_0\mathbf{x} = \mathbf{A}\boldsymbol{\theta}' + \mathbf{B}\dot{\boldsymbol{\theta}}' \tag{1}$$

$$\mathbf{J}\ddot{\boldsymbol{\theta}} + \mathbf{C}\dot{\boldsymbol{\theta}} + \mathbf{K}\boldsymbol{\theta} = \mathbf{M} + \mathbf{A}'\mathbf{Y} + \mathbf{B}'\dot{\mathbf{Y}} \tag{2}$$

where

$$\mathbf{m} = \operatorname{diag}[m_1 \ m_2 \ m_3 \ m_4 \ m_1 \ m_2 \ m_3 \ m_4]$$

$$\mathbf{x} = [x_1 \ x_2 \ x_3 \ x_4 \ y_1 \ y_2 \ y_3 \ y_4]^T$$

$$\boldsymbol{\theta}' = [0 \ 0 \ 0 \ 0 \ \theta_1 \ \theta_2 \ \theta_3 \ \theta_4]^T$$

$$\mathbf{c_0} = \begin{bmatrix} c_{x1} & 0 & 0 & 0 & 0 & 0 & 0 & 0 \\ 0 & c_{x2} & 0 & 0 & 0 & 0 & 0 & 0 \\ 0 & 0 & c_{x3} & 0 & 0 & 0 & 0 & 0 \\ 0 & 0 & 0 & c_{x4} & 0 & 0 & 0 & 0 \\ 0 & 0 & 0 & 0 & c_{y1}+c_{t1} & -c_{t1} & 0 & 0 \\ 0 & 0 & 0 & 0 & -c_{t1} & c_{y2}+c_{t1} & 0 & 0 \\ 0 & 0 & 0 & 0 & 0 & 0 & c_{y3}+c_{t2} & -c_{t2} \\ 0 & 0 & 0 & 0 & 0 & 0 & -c_{t2} & c_{y4}+c_{t2} \end{bmatrix}$$

$$\mathbf{k_0} = \begin{bmatrix} k_{x1} & 0 & 0 & 0 & 0 & 0 & 0 & 0 \\ 0 & k_{x2} & 0 & 0 & 0 & 0 & 0 & 0 \\ 0 & 0 & k_{x3} & 0 & 0 & 0 & 0 & 0 \\ 0 & 0 & 0 & k_{x4} & 0 & 0 & 0 & 0 \\ 0 & 0 & 0 & 0 & k_{y1}+k_{t1} & -k_{t1} & 0 & 0 \\ 0 & 0 & 0 & 0 & -k_{t1} & k_{y2}+k_{t1} & 0 & 0 \\ 0 & 0 & 0 & 0 & 0 & 0 & k_{y3}+k_{t2} & -k_{t2} \\ 0 & 0 & 0 & 0 & 0 & 0 & -k_{t2} & k_{y4}+k_{t2} \end{bmatrix}$$

$$\mathbf{A} = \begin{bmatrix} 0 & 0 & 0 & 0 & 0 & 0 & 0 & 0 \\ 0 & 0 & 0 & 0 & 0 & 0 & 0 & 0 \\ 0 & 0 & 0 & 0 & 0 & 0 & 0 & 0 \\ 0 & 0 & 0 & 0 & 0 & 0 & 0 & 0 \\ 0 & 0 & 0 & 0 & -k_{t1}r_{b1} & k_{t1}r_{b2} & 0 & 0 \\ 0 & 0 & 0 & 0 & -k_{t1}r_{b1} & k_{t1}r_{b2} & 0 & 0 \\ 0 & 0 & 0 & 0 & 0 & 0 & -k_{t2}r_{b3} & k_{t2}r_{b4} \\ 0 & 0 & 0 & 0 & 0 & 0 & -k_{t2}r_{b3} & k_{t2}r_{b4} \end{bmatrix}$$

$$\mathbf{B} = \begin{bmatrix} 0 & 0 & 0 & 0 & 0 & 0 & 0 & 0 \\ 0 & 0 & 0 & 0 & 0 & 0 & 0 & 0 \\ 0 & 0 & 0 & 0 & 0 & 0 & 0 & 0 \\ 0 & 0 & 0 & 0 & 0 & 0 & 0 & 0 \\ 0 & 0 & 0 & 0 & -c_{t1}r_{b1} & c_{t1}r_{b2} & 0 & 0 \\ 0 & 0 & 0 & 0 & -c_{t1}r_{b1} & c_{t1}r_{b2} & 0 & 0 \\ 0 & 0 & 0 & 0 & 0 & 0 & -c_{t2}r_{b3} & c_{t2}r_{b4} \\ 0 & 0 & 0 & 0 & 0 & 0 & -c_{t2}r_{b3} & c_{t2}r_{b4} \end{bmatrix} \quad (3)$$

where

$$\mathbf{J} = \operatorname{diag}\begin{bmatrix} J_0 & J_1 & J_2 & J_3 & J_4 & J_5 \end{bmatrix}$$

$$\boldsymbol{\theta} = \begin{bmatrix} \theta_0 & \theta_1 & \theta_2 & \theta_3 & \theta_4 & \theta_5 \end{bmatrix}^T$$

$$\mathbf{M} = \begin{bmatrix} M_0 & 0 & 0 & 0 & 0 & M_5 \end{bmatrix}^T$$

$$\mathbf{K} = \begin{bmatrix} k_1 & -k_1 & 0 & 0 & 0 & 0 \\ -k_1 & k_1 + r_{b1}k_{t1}r_{b1} & -r_{b1}k_{t1}r_{b2} & 0 & 0 & 0 \\ 0 & -r_{b2}k_{t1}r_{b1} & k_2 + r_{b2}k_{t1}r_{b2} & -k_2 & 0 & 0 \\ 0 & 0 & -k_2 & k_2 + r_{b3}k_{t2}r_{b3} & -r_{b3}k_{t2}r_{b4} & 0 \\ 0 & 0 & 0 & -r_{b4}k_{t2}r_{b3} & k_3 + r_{b4}k_{t2}r_{b4} & -k_3 \\ 0 & 0 & 0 & 0 & -k_3 & k_3 \end{bmatrix}$$

$$\mathbf{C} = \begin{bmatrix} c_1 & -c_1 & 0 & 0 & 0 & 0 \\ -c_1 & c_1 + r_{b1}c_{t1}r_{b1} & -r_{b1}c_{t1}r_{b2} & 0 & 0 & 0 \\ 0 & -r_{b2}c_{t1}r_{b1} & c_2 + r_{b2}c_{t1}r_{b2} & -c_2 & 0 & 0 \\ 0 & 0 & -c_2 & c_2 + r_{b3}c_{t2}r_{b3} & -r_{b3}c_{t2}r_{b4} & 0 \\ 0 & 0 & 0 & -r_{b4}c_{t2}r_{b3} & k_3 + r_{b4}c_{t2}r_{b4} & -c_3 \\ 0 & 0 & 0 & 0 & -c_3 & c_3 \end{bmatrix}$$

$$\mathbf{A}' = \begin{bmatrix} 0 & 0 & 0 & 0 & 0 & 0 \\ 0 & -r_{b1}k_{t1} & 0 & 0 & 0 & 0 \\ 0 & 0 & r_{b2}k_{t1} & 0 & 0 & 0 \\ 0 & 0 & 0 & -r_{b3}k_{t2} & 0 & 0 \\ 0 & 0 & 0 & 0 & r_{b4}k_{t2} & 0 \\ 0 & 0 & 0 & 0 & 0 & 0 \end{bmatrix}$$

$$\mathbf{B}' = \begin{bmatrix} 0 & 0 & 0 & 0 & 0 & 0 \\ 0 & -r_{b1}c_{t1} & 0 & 0 & 0 & 0 \\ 0 & 0 & r_{b2}c_{t1} & 0 & 0 & 0 \\ 0 & 0 & 0 & -r_{b3}c_{t2} & 0 & 0 \\ 0 & 0 & 0 & 0 & r_{b4}c_{t2} & 0 \\ 0 & 0 & 0 & 0 & 0 & 0 \end{bmatrix}$$

$$\mathbf{Y} = \begin{bmatrix} 0 \\ y_1 - y_2 - e_{t1} \\ y_1 - y_2 - e_{t1} \\ y_3 - y_4 - e_{t2} \\ y_3 - y_4 - e_{t2} \\ 0 \end{bmatrix} \tag{4}$$

where

m_i is the quality of each gear, $i = 1, 2, 3, 4$;

r_{bi} is the base radius of each gear, $i = 1, 2, 3, 4$;

J_i is the moment of inertia of each gear, $i = 1, 2, 3, 4$;

J_0, J_5 are the moment of inertia of motor and load;

M_0, M_5 are the input torque of motor and load resistance torque;

k_i, c_i are the torsional stiffness and damping coefficient of input, mid, and output axes, $i = 1, 2, 3$;

k_{xi}, k_{yi} are the radial stiffness of x-axis and y-axis direction of each bearing, $i = 1, 2, 3, 4$;

c_{xi}, c_{yi} are the damping coefficient of x-axis and y-axis direction of each bearing, $i = 1, 2, 3, 4$;

x_i, y_i are the displacement of x-axis and y-axis direction of each bearing, $i = 1, 2, 3, 4$;

θ_i is the rotation angular displacement of input axis, each gear and output axis, $i = 0, 1, 2, 3, 4, 5$;

e_{ti} is the transmission error of gear pair i, $i = 1, 2$;

k_{ti} is the linear time-varying meshing stiffness of gear pair i, $i = 1, 2$;

c_{ti} is the linear time-varying damping coefficient of gear pair i, $i = 1, 2$.

3. Profile Error and Index Error

Affected by gear machining and machine tool accuracy, a certain deviation exists between the actual and the theoretical tooth profile. The actual tooth surface error of spur gear constitutes a comprehensive error, which can be broken down into multiple errors as PE (involute tilt deviation $f_{H\alpha}$ and form deviation $f_{f\alpha}$) and IE. In this case, based on the gear meshing theory, with the PE and IE consideration as an example, the impact on the transmission error was studied. Both PE and IE are presented in Figure 3.

3.1. Profile Error. The PE of a tooth could be deduced and consequently expanded into a periodic function, which approximates the tooth profile deviation. Mucchi et al. [22] proposed an equation for the tooth profile deviations descriptions, as presented in

$$e_{PE}(s) = f_{h\alpha}\frac{s - s_0}{s_f - s_0} + \frac{f_{f\alpha}}{2}\sin\left(2\pi f_r \frac{s - s_0}{s_f - s_0}\right) \tag{5}$$

where

s is the roll path length;

s_f is the maximum curvature radius of tooth profile;

s_0 is the minimum curvature radius of tooth profile;

f_r is the ratio of total length of each tooth profile and cycle of PE.

With the $f_{h\alpha}$ and $f_{f\alpha}$ consideration for the PE tolerance, the specific values could be observed in Table 1. To simplify the calculation, the f_r was taken as 1. With a randomly initial phase given, according to Table 1 and (5), the PE curve of four gears could be obtained, as presented in Figure 4.

3.2. Index Error. The IE was different from the PE, while the IE of each tooth was a fixed constant. Therefore, the IE was discretized and periodic, which can be expressed as the sum of the nth harmonic, as presented in the following equation [17]:

$$e_{pt}(\theta) = \sum_{n=1}^{N} A_n \sin\left(n \cdot floor\left(\frac{\theta}{\theta_p}\right) \cdot \theta_p\right), \quad \theta_p = \frac{2\pi}{Z} \tag{6}$$

where

n is the number of harmonics;

θ is the angle of rotation of gear;

Z is the teeth number of gear;

A_n is the amplitude of IE.

The *floor* function constitutes a discrete function, which could return the highest integer that was less than or equal to the specified expression. In this manner, the IE of each tooth in the gear could be obtained. With A_n as the tolerance of

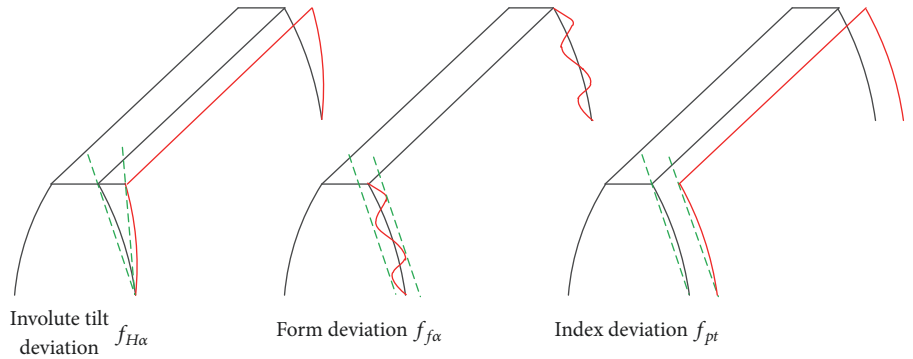

Figure 3: Diagrams of PE and IE.

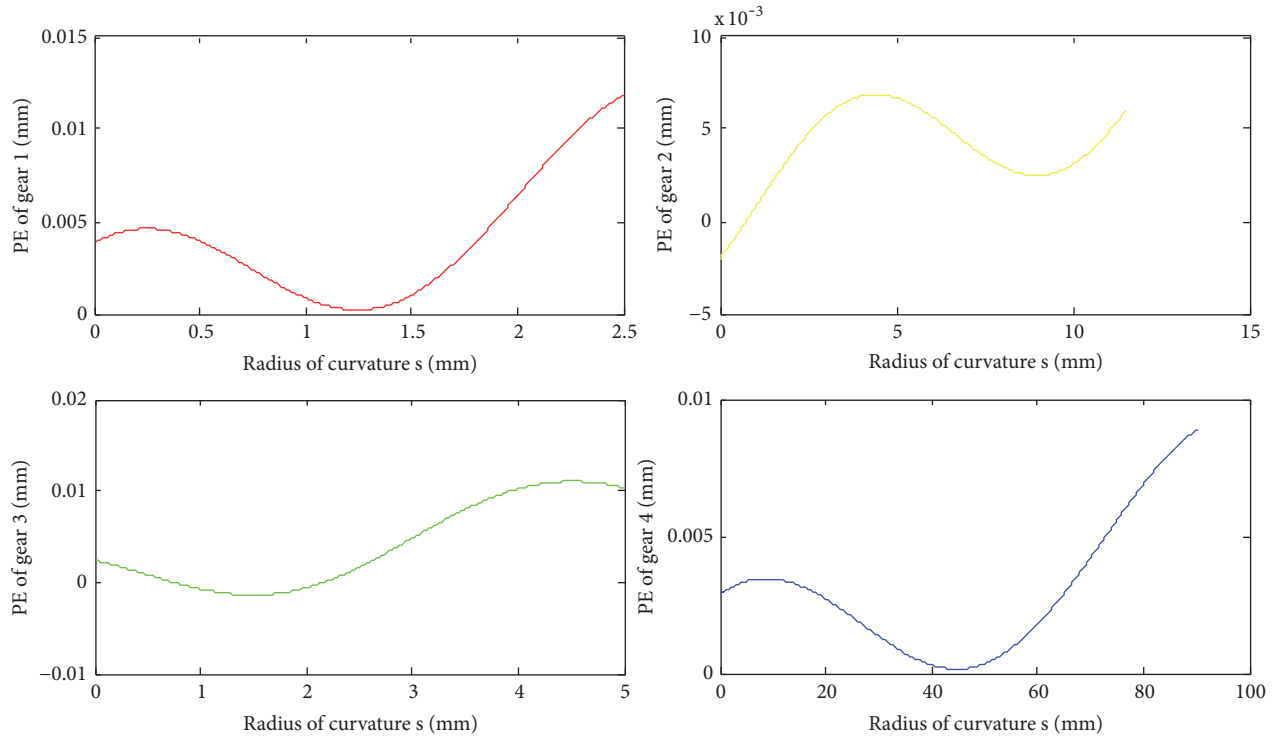

Figure 4: PE curves of four gears.

cycle accumulated deviations consideration, the specific values could be observed in Table 1. To simplify the calculation, for the IE in this paper, the first harmonic was considered only. Given an initial phase randomly, according to (6), the IE curve of four gears could be obtained, as presented in Figure 5.

4. Static Analysis

To produce a preliminary evaluation of the two-stage spur-space-driven characteristic mechanism, the gear system was first analyzed statically.

To compare the effects of PE and IE on the overall transmission error of the gear system, only one of the deviations was considered, whereas the time-domain and frequency-domain curves of the TE were obtained, as presented in Figure 6. The amplitude of the TE was low when the PE was considered only, whereas the spectrum was mainly concentrated on the gear meshing frequency and the corresponding frequency multiplication. The amplitude of the TE was higher when the IE was considered only, whereas the spectrum was mainly concentrated on the gear rotation frequency, the gear meshing frequency, and the corresponding frequency multiplication. According to the TE spectrum and time-domain curve, it was easy to identify the two types of errors.

For the effects comparison of gear pairs 1 and 2 on the TE of the gear system, the static simulation was considered in each one and the TE curve was obtained, as presented in

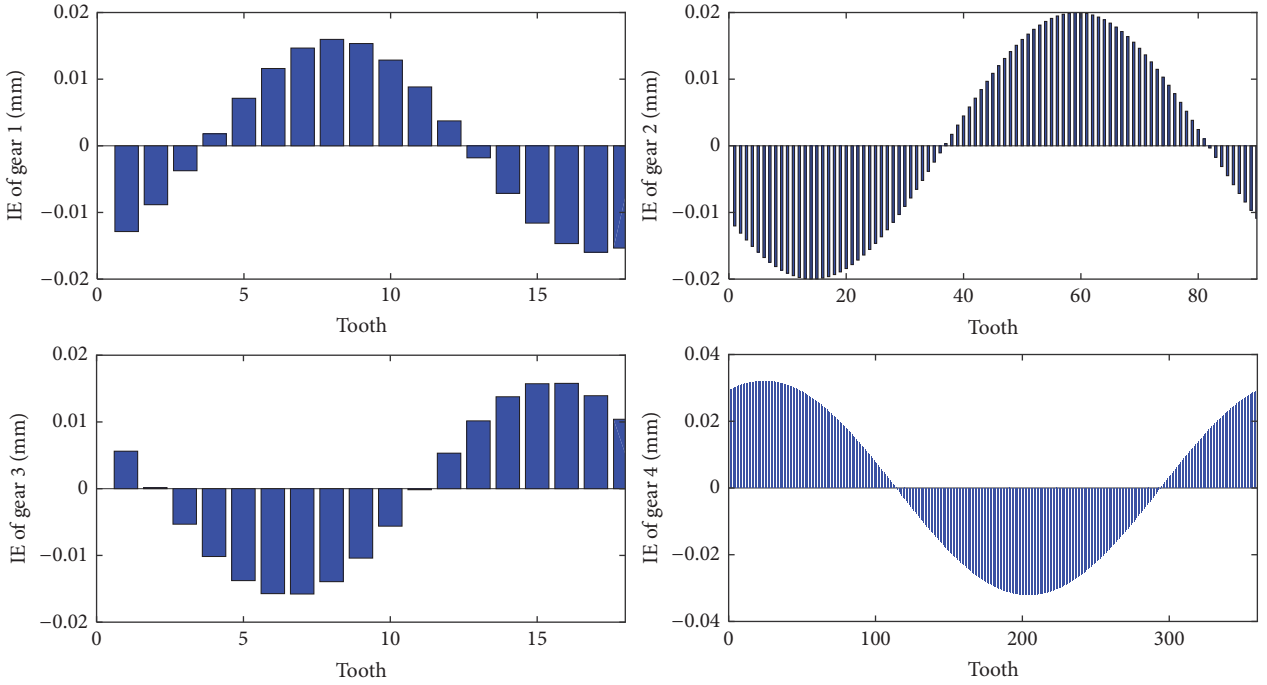

Figure 5: IE curves of four gears.

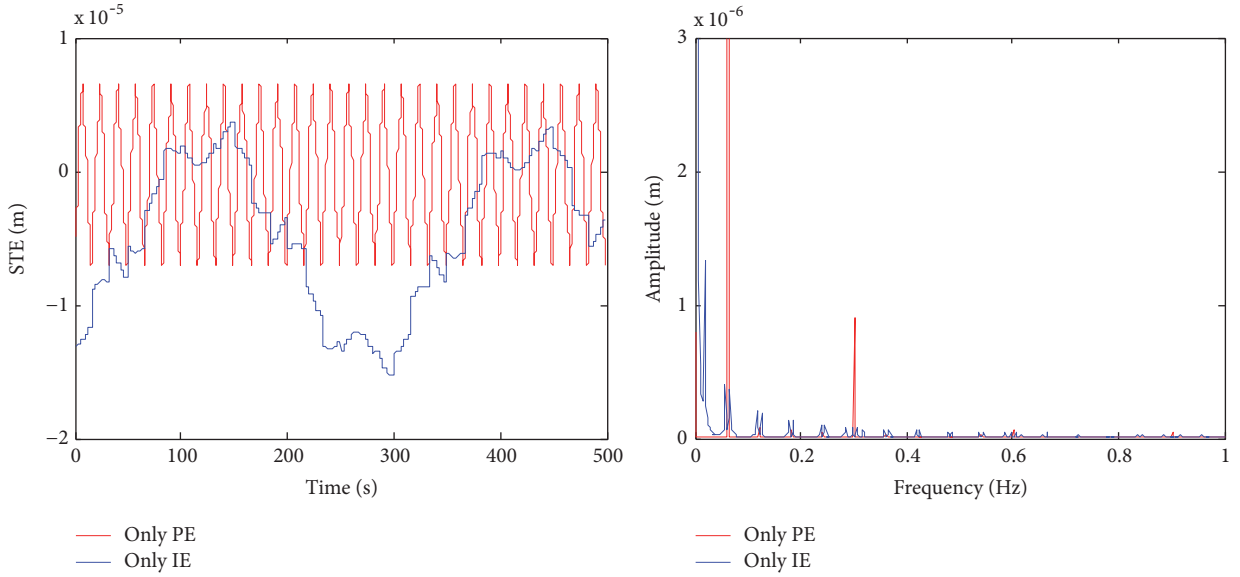

Figure 6: Effects of PE and IE on overall transmission error of gear system.

Figure 7. The amplitude change of gear pair 2 was significantly pronounced compared to gear pair 1. Consequently, the gear pair 2 would cause system disturbance quite easily.

5. Dynamic Analysis

The dynamic simulation results of LTE under the default speed and load torque are presented in Figure 8, simultaneously compared to static simulation results. The LTE curves obtained by the two simulation methods were basically the same in the trend, whereas the amplitude of dynamic simulation was an order of magnitude higher than the static simulation amplitude. The DTE curve contained additional information and the waveform was significantly complex, because the dynamic model contained the factors of backlash, time-varying stiffness, friction, and damping. Certain fluctuations in the STE became less noticeable in the DTE, because the large inertia load had the capability to absorb the disturbance. Consequently, the transmission error curve became smooth. Therefore, a big difference existed between

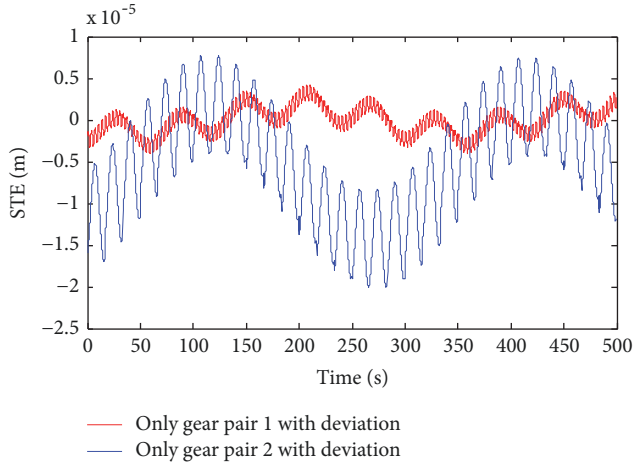

Figure 7: Effects comparison of two gear pairs on TE.

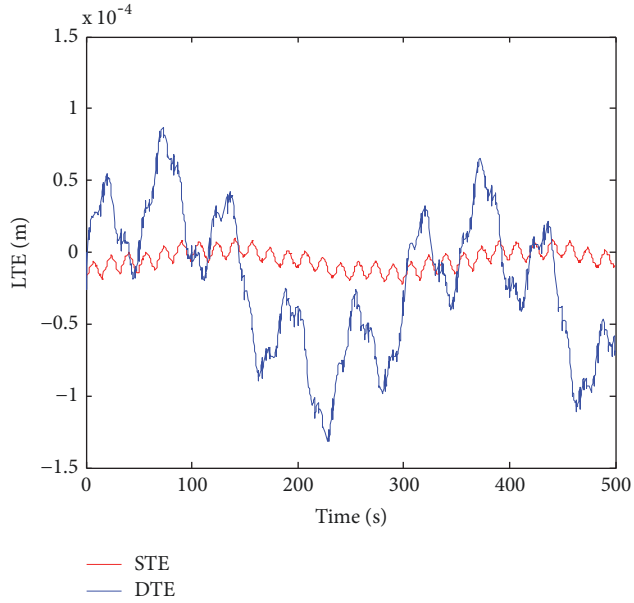

Figure 8: Comparison of DTE and STE.

the dynamic and static simulations. Subsequently, it was necessary for the dynamic simulation analysis of the gear system to be conducted.

5.1. LTE at Different Torque. In this paper, the study of large inertia load space drive mechanism gear system was utilized for the satellite sun wing drive. Due to the sun wing requirement for the angle change according to the sun's position in real time, this mechanism was required to start and stop frequently at low speed. The inertia of the solar wing was high, so the load torque of the system was required to frequently change during the operation. This was the cause of the gear system disturbance. Therefore, it was necessary to analyze the load torque of this mechanism. The LTE curves under different torques were compared, as presented in Figure 9.

It could be observed from Figure 9 that the cyclical change trend of the load transmission error under different torques is the same. As the torque increased, the amplitude of the load transmission error shifted downwards. This was consistent with the results in the literature [18]. This verified the correctness of the dynamics model. In literature [18], it was mentioned that the increase in load torque increased the peak-to-peak value of LTE, which was not apparent in this case. This occurred due to the low rated load torque.

From the aforementioned analysis, the load torque change had a high effect on the LTE. The dynamic simulation of the variable load torque was executed for further analysis. In the premise of ensuring that the average load torque was constant, the linearly varying torque F_l and the sinusoidal variation of the torque Fs were simulated, as presented in (7) and (8) (sinusoidal parameters taken separately $A = 0.05Nm$

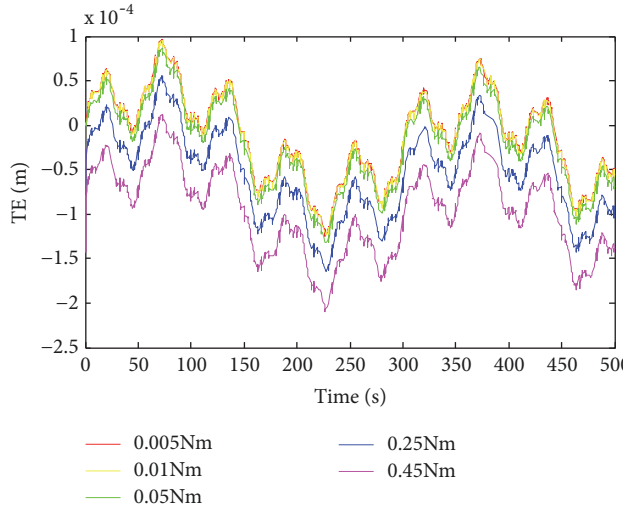

Figure 9: LTE curves under different torques.

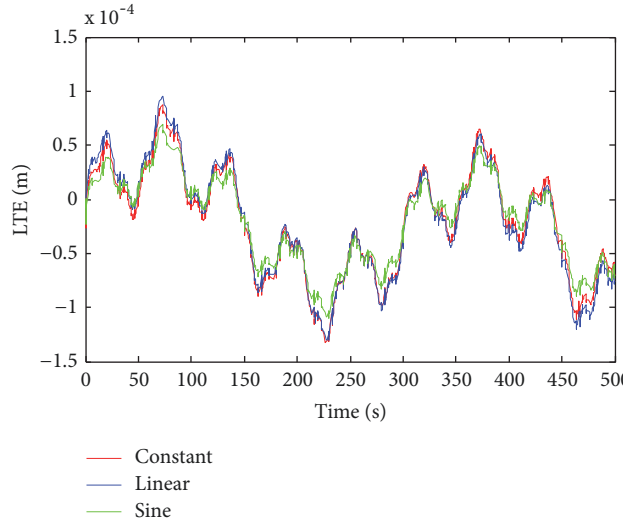

Figure 10: LTE curves under variable load torques.

and $f = 1/2\pi$). The simulation results were compared to the LTE under default torque, as presented in Figure 10. The linearly varying torque and the fixed torque transmission error curve were basically the same; the change was not apparent, whereas the sinusoidal variation of torque significantly reduced the overall peak-to-peak value of the LTE. The load torque was affected by the input torque. Consequently, the change of the load torque could be achieved by changing the input torque in the practical application.

$$F_l = \frac{2F_d\theta_i}{t_m} \tag{7}$$

$$Fs = A\sin\left(2\pi f\theta_i\right) + F_d \tag{8}$$

where

F_d is the default load torque;

θ_i is the rotation angle of input shaft;

t_m is the simulation time;

A is the amplitude of sine load torque;

f is the frequency of sine load torque.

From the aforementioned analysis, it could be observed that the sine-changing load contributed in the LTE amplitude reduction and reduced the disturbance of the gear system. In order to obtain the optimal scheme, the sine change scheme under different parameters was compared, as presented in Figures 11–14.

In Figure 11, the amplitude of the sine load torque was changed in the case of ensuring that the load torque average and the frequency were constant (frequency taken as $f = 1/2\pi$). Since many curves existed, it was not significantly apparent. To make the results more intuitive, the peak-to-peak value of the LTE at different amplitudes was extracted, as presented in Figure 12. It could be observed from Figure 12 that the overall peak-to-peak value of the LTE decreased

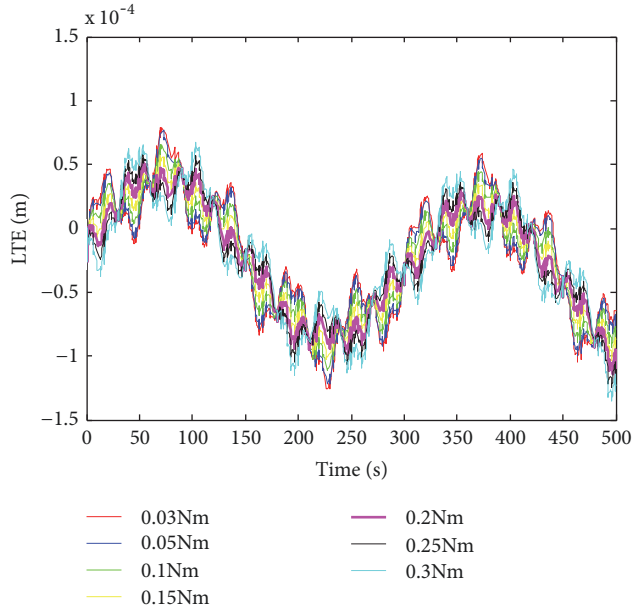

Figure 11: LTE curves under different amplitudes of sine load torque.

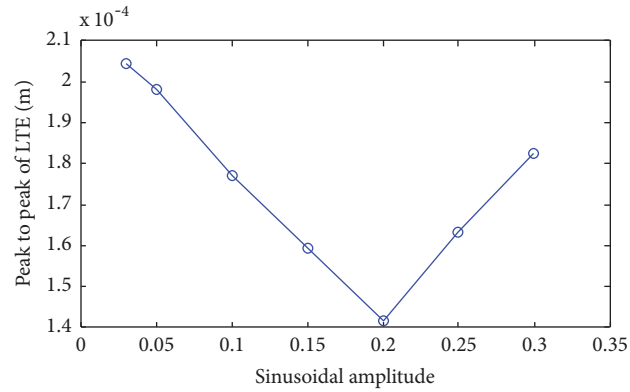

Figure 12: Peak-to-peak value of LTE under different amplitudes of sine load torque.

first and then increased as the amplitude increased. When the amplitude of the sinusoidal load torque was 0.2 Nm, the overall peak-to-peak value of the LTE was minimized.

The amplitude remained at 0.2 Nm and the frequency of sine load torque changed. First, the rotation frequency of the input axis was selected, along with the middle axis and the meshing frequency of gear pairs 1 and 2. Then, the frequency was selected at $1/8\pi$, $1/4\pi$, $1/\pi$, and $2/\pi$, where, respectively, it was compared to $f = 1/2\pi$. Through the LTE comparison under various parameters, the $f = 1/2\pi$ was the best frequency and the overall peak-to-peak value of the LTE was the lowest, as presented in Figures 13 and 14.

5.2. Effect of PE and IE Parameter Changes on LTE. From the static analysis of Part 3, it could be observed that gear pair 2 was more likely to cause the disturbance of the gear system. In order to simplify the calculation, the error of gear pair 2 was considered only. Respectively, as the amplitude parameters of PE and IE increased or decreased, the LTE curves are presented in Figure 15.

As it could be observed from Figure 15, the IE affected the overall amplitude of LTE. Although the IE reduction reduced the DTE magnitude, a slight impact on the number of fluctuations existed. The PE reduction significantly reduced the volatility number of the DTE, which contributed to the disturbance reduction of the gear system. In the actual design of the gear system process it is possible to reduce PE through the gear accuracy level improvement.

6. Optimum Design Scheme of Gear System with Large Inertia Load

According to the static and dynamic analyses, the optimal design scheme was put forward. The default accuracy level was 6-h, which could be observed from Table 1. The accuracy level of gear pair 2 was increased to 5-h and the partial

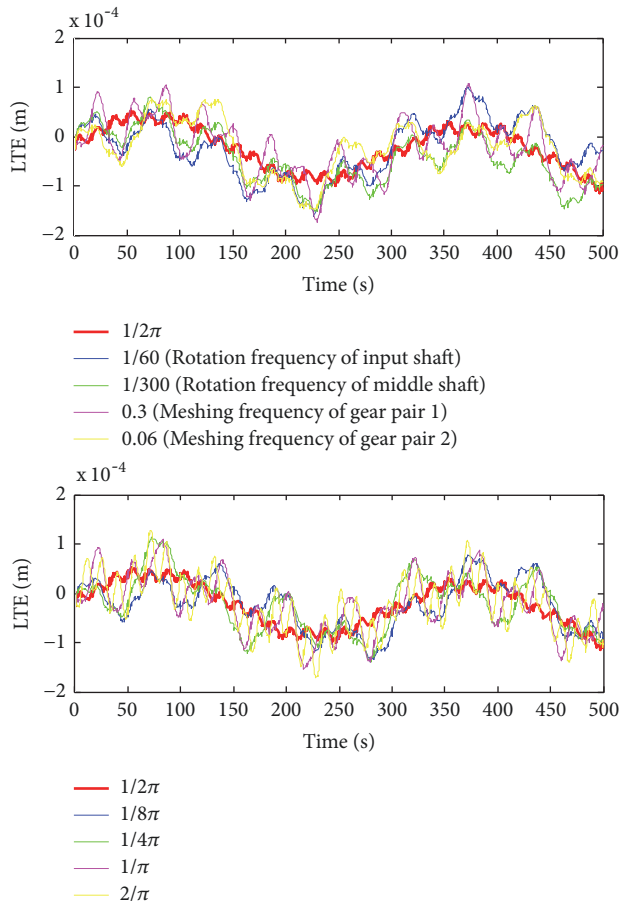

Figure 13: LTE curves under different frequencies of sine load torque.

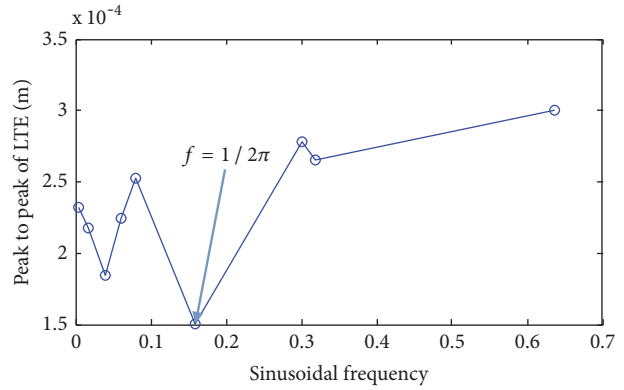

Figure 14: Peak-to-peak value of LTE under different frequencies of sine load torque.

parameters of gear pair 2 are presented in Table 2. Through the input torque control, the load torque changed as presented in (8) in the sine form, where the sine parameters were taken as $A = 0.2Nm$, $f = 1/2\pi$, and $F_d = 0.05Nm$.

The DTE values of the load prior to and following optimization were compared, as presented in Figures 16 and 17. The overall peak-to-peak value of LTE of the optimized gear system was reduced by 60.7%, which improved the gear system transmission accuracy of the space drive mechanism. In the frequency domain presented in Figure 17, the frequencies corresponding to the numbers 1 to 5 represented the rotation frequency values of the intermediate shaft, the intermediate shaft double frequency, the rotation frequency of the input shaft, the meshing frequency of gear pair 2, and the meshing frequency of gear pair 1. The amplitudes of the rotation frequency of the input shaft, the rotation frequency of the intermediate shaft, and the corresponding double frequency were high before optimization, which was the main cause

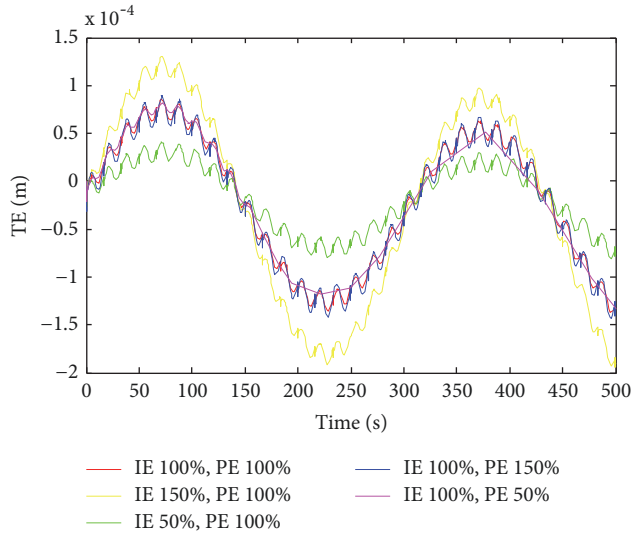

Figure 15: Effect of the amplitude parameters of PE and IE on LTE.

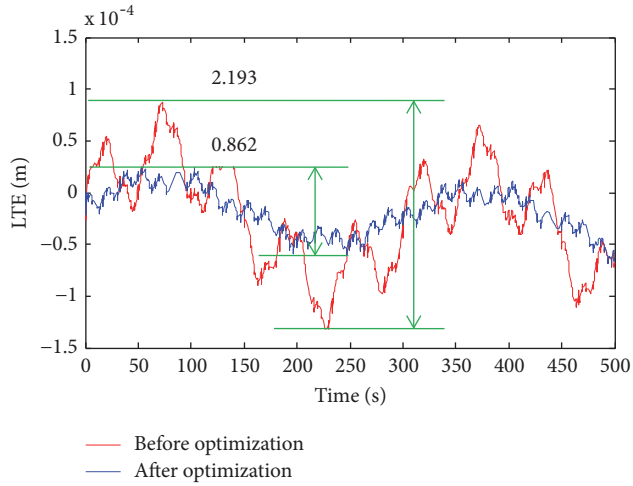

Figure 16: Time-domain comparison of LTE prior to and following optimization.

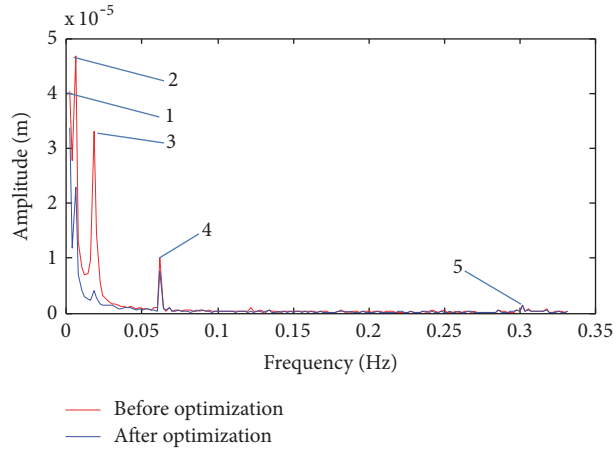

Figure 17: Frequency-domain comparison of LTE prior to and following optimization.

Table 2: Optimized gear parameters.

Accuracy level	5-h
Tolerance of cycle accumulated deviations of gear 3	0.011mm
Tolerance of cycle accumulated deviations of gear 4	0.022mm
Tolerance of PE of gear 3	0.006mm
Tolerance of PE of gear 4	0.004mm

of the disturbance phenomenon. Following optimization, the amplitudes of these frequencies were highly reduced, where the rotation frequency of the input shaft decreased the most. The meshing frequency of gear pair 2 itself was not high, which was slightly reduced after optimization. The amplitude of the meshing frequency of gear pair 1 was too low to be apparent in the figure. The amplitude-frequency curves prior to and following optimization demonstrated that the optimization scheme could effectively reduce the disturbance of the gear system.

7. Conclusions

(1) A nonlinear dynamic model of 14-DOF motion of spur gear with time-varying meshing stiffness and damping was established for the study of LTE, which included the torsional displacement vibration in 6 directions and the radial displacement vibration in 8 directions.

(2) The PE and IE were extended in the dynamic model, whereas the static analysis of the gear system was executed. The results demonstrated that the amplitude difference of the TE caused by gear pair 2 was significantly apparent compared to gear pair 1, which was more likely to cause the system disturbance.

(3) The dynamic analysis of the gear system was executed and the TE under different load torques was compared. The results demonstrated that the load torque had a high effect on the TE of the gear system. When the load torque changed to the sinusoidal form, the overall peak-to-peak value of LTE was minimal. The LTE values of different sine parameters were compared and the optimal parameters are obtained.

(4) According to the results of static and dynamic simulations, the optimal design scheme was put forward. The optimized TE curve was compared to the TE curve before optimization, whereas the overall peak-to-peak value of the transmission error was reduced by 60.7%, which in turn improved the transmission accuracy and reduced the disturbance phenomenon.

(5) In this paper, the nonlinear dynamic model research of the two-stage spur gear and large inertia load TE was enriched, providing an important reference for the actual design of the gear system. In further study, the correctness of the optimization scheme will be verified through experiments and some advanced signal processing methods in the analysis of gearboxes would be considered.

Nomenclature

PE: Profile error
IE: Index error
TE: Transmission error
DOF: Degree of freedom
LTE: Load transmission error
STE: Static transmission error
DTE: Dynamic transmission error.

Conflicts of Interest

The authors declare that they have no conflicts of interest.

Acknowledgments

This work was supported by the National Natural Science Foundation of China (51575007) and the Municipal Education Commission project of Beijing (JC001011201601).

References

[1] L. Cui, N. Wu, C. Ma, and H. Wang, "Quantitative fault analysis of roller bearings based on a novel matching pursuit method with a new step-impulse dictionary," *Mechanical Systems and Signal Processing*, vol. 68-69, pp. 34–43, 2016.

[2] L. Cui, J. Huang, and F. Zhang, "Quantitative and localization diagnosis of a defective ball bearing based on vertical-horizontal synchronization signal analysis," *IEEE Transactions on Industrial Electronics*, vol. 64, no. 11, pp. 8695–8706, 2017.

[3] L. Cui, J. Wang, and S. Lee, "Matching pursuit of an adaptive impulse dictionary for bearing fault diagnosis," *Journal of Sound and Vibration*, vol. 333, no. 10, pp. 2840–2862, 2014.

[4] L. Cui, J. Huang, H. Zhai, and F. Zhang, "Research on the meshing stiffness and vibration response of fault gears under an angle-changing crack based on the universal equation of gear profile," *Mechanism and Machine Theory*, vol. 105, pp. 554–567, 2016.

[5] J. Wang, G. He, J. Zhang, Y. Zhao, and Y. Yao, "Nonlinear dynamics analysis of the spur gear system for railway locomotive," *Mechanical Systems and Signal Processing*, vol. 85, pp. 41–55, 2017.

[6] L. Walha, T. Fakhfakh, and M. Haddar, "Nonlinear dynamics of a two-stage gear system with mesh stiffness fluctuation, bearing flexibility and backlash," *Mechanism and Machine Theory*, vol. 44, no. 5, pp. 1058–1069, 2009.

[7] K. Abboudi, L. Walha, Y. Driss, M. Maatar, T. Fakhfakh, and M. Haddar, "Dynamic behavior of a two-stage gear train used in a fixed-speed wind turbine," *Mechanism and Machine Theory*, vol. 46, no. 12, pp. 1888–1900, 2011.

[8] R. G. Parker, V. Agashe, and S. M. Vijayakar, "Dynamic response of a planetary gear system using a finite element/contact mechanics model," *Journal of Mechanical Design*, vol. 122, no. 3, pp. 304–310, 2000.

[9] R. G. Parker, S. M. Vijayakar, and T. Imajo, "Non-linear dynamic response of a spur gear pair: modelling and experimental

comparisons," *Journal of Sound and Vibration*, vol. 237, no. 3, pp. 435–455, 2000.

[10] F. D. A. Rincon, F. Viadero, M. Iglesias et al., "A model for the study of meshing stiffness in spur gear transmissions," *Mechanism & Machine Theory*, vol. 61, no. 61, pp. 30–58, 2013.

[11] Y.-J. Wu, J.-J. Wang, and Q.-K. Han, "Contact finite element method for dynamic meshing characteristics analysis of continuous engaged gear drives," *Journal of Mechanical Science and Technology*, vol. 26, no. 6, pp. 1671–1685, 2012.

[12] L. Cui, H. Zhai, and F. Zhang, "Research on the meshing stiffness and vibration response of cracked gears based on the universal equation of gear profile," *Mechanism and Machine Theory*, vol. 94, pp. 80–95, 2015.

[13] T. Yang, S. Yan, and Z. Han, "Nonlinear model of space manipulator joint considering time-variant stiffness and backlash," *Journal of Sound and Vibration*, vol. 341, pp. 246–259, 2015.

[14] Z. Xu, X. Bai, M. Yang, and J. Wang, "Load equivalent simulation method of ultra-large moment of inertia of space station redocking manipulator," *Journal of Information and Computational Science*, vol. 12, no. 2, pp. 431–441, 2015.

[15] C. Shiqi, Z. Jiyun, L. Bingwen, X. Zhan, and F. Yanqiu, "Nonlinear dynamic model and governing equations of low speed and high load planetary gear train with respect to friction," in *Proceedings of the International Conference on Consumer Electronics, Communications and Networks*, XianNing, China, April 2011.

[16] A. Hammami, F. D. A. Rincon, F. Chaari et al., "Effects of variable loading conditions on the dynamic behaviour of planetary gear with power recirculation," *Measurement*, vol. 94, pp. 306–315, 2016.

[17] A. Fernández-del-Rincón, M. Iglesias, A. De-Juan, A. Diez-Ibarbia, P. García, and F. Viadero, "Gear transmission dynamics: effects of index and run out errors," *Applied Acoustics*, vol. 108, pp. 63–83, 2016.

[18] A. Fernández, M. Iglesias, A. De-Juan, P. García, R. Sancibrián, and F. Viadero, "Gear transmission dynamic: effects of tooth profile deviations and support flexibility," *Applied Acoustics*, vol. 77, pp. 138–149, 2014.

[19] M. A. Hotait and A. Kahraman, "Experiments on the relationship between the dynamic transmission error and the dynamic stress factor of spur gear pairs," *Mechanism and Machine Theory*, vol. 70, pp. 116–128, 2013.

[20] T. Lin and Z. He, "Analytical method for coupled transmission error of helical gear system with machining errors, assembly errors and tooth modifications," *Mechanical Systems and Signal Processing*, vol. 91, pp. 167–182, 2017.

[21] W. Guangjian, C. Lin, Y. Li, and Z. Shuaidong, "Research on the dynamic transmission error of a spur gear pair with eccentricities by finite element method," *Mechanism and Machine Theory*, vol. 109, pp. 1–13, 2017.

[22] J. Ma, C. Li, Y. Luo, and L. Cui, "Nonlinear dynamic response analysis of two-stage spur gear space driving mechanism with large inertia load," *Journal of Vibroengineering*, vol. 20, no. 1, pp. 86–102, 2018.